

Dynamic State Estimation for Wind Turbine Models with Unknown Wind Velocity

Georgios Anagnostou, *Member, IEEE*, Linash P. Kunjumammed, *Senior Member, IEEE*, and Bikash C. Pal, *Fellow, IEEE*

Abstract—This paper proposes a novel Kalman filtering based dynamic state estimation method, which addresses cases of models with a nonlinear unknown input, and it is suitable for wind turbine model state estimation. Given the complexity characterising modern power networks, dynamic state estimation techniques applied on renewable energy based generators, such as wind turbines, enhance operators' awareness of the components comprising modern power networks. In this context, the method developed here is implemented on a doubly-fed induction generator based wind turbine, under unknown wind velocity conditions, as opposed to similar studies so far, where all model inputs are considered to be known, and this does not always reflect the reality. The proposed technique is derivative-free and it relies on the formulation of the nonlinear output measurement equations as power series. The effectiveness of the suggested algorithm is tested on a modified version of the IEEE benchmark 68-bus, 16-machine system.

Index Terms—Doubly-fed induction generators, Dynamic state estimation, Kalman filtering, unknown inputs, wind turbines

I. INTRODUCTION

ELECTRIC power systems all over the world are undergoing significant changes, mainly driven by energy market liberalisation taking place in various countries, as well as the advent of renewable energy based power generators [1], [2]. The adoption of new technologies introduces complexity in terms of network control and operation, therefore, good knowledge of the behavioural model characterising the newly introduced devices is challenging but very important. On the other hand, the longstanding operation of power networks is associated with the existence of aging components which are likely to increase system stress and put system operation at risk, with a notable example being the 1994 North American blackouts in WECC [2], [3].

Given the aforementioned modern network challenges, dynamic security assessment (DSA) and wide area monitoring systems (WAMS) are useful approaches, providing insight regarding the system behaviour with respect to the advent of contingencies [4]. In this context, dynamic state estimation (DSE) is a useful tool to monitor the operational status of the system. DSE is model-based, thus, good knowledge of

This work has been supported by the U.K.–China initiative in Stability and Control of Power Networks with Energy Storage (STABLE-NET), and the Joint UK-India Clean Energy Centre (JUICE), both funded by the Research Council U.K. (RCUK) Energy Programme (contract numbers: EP/L014343/1 & EP/P003605/1, respectively).

G. Anagnostou, L. P. Kunjumammed, and B. C. Pal are with the Department of Electrical and Electronic Engineering, Imperial College London SW7 2AZ, U.K. (e-mails: anagnostou.georgios@gmail.com; linash.p.k@imperial.ac.uk; b.pal@imperial.ac.uk)

the devices comprising the power network under study is fundamental, in order to obtain highly accurate results. In this respect, various DSE methods have been proposed in power systems literature, engaging primarily Kalman filter variants, such as the Extended Kalman filter (EKF) and the Unscented Kalman filter (UKF), addressing the nonlinear features of electric power systems [5]–[9].

Kalman filtering based DSE studies have primarily been devoted to synchronous generators, and various techniques have been proposed, addressing cases when complete model information is required, or the estimation is conducted under the presence of unknown inputs [5]–[9]. Moreover, such algorithms have started to be implemented in renewable energy based generators, such as fuel cells [10], [11] and wind turbine generators (WTGs) [12]–[15]. However, in the context of the latter case, the DSE is performed under the assumption that all inputs, including the wind velocity, are known, which is not always achievable in practice.

To tackle this issue, the work conducted in [8] is extended so as to perform DSE of a wind turbine, when the wind velocity is unknown or uncertain, assuming no prior knowledge of the unknown input models or distributions. Here, the method proposed has been modified in such a way so as to address the nonlinearity which characterises the unknown input (i.e. the wind velocity), since the technique proposed in [8] deals with additive unknown inputs only. This research effort leads to the following contributions:

- to propose a novel derivative-free Kalman filtering based estimator, for models with a nonlinear unknown input;
- to establish a dynamic state estimation framework for doubly-fed induction generator (DFIG) based wind turbine models under uncertain wind velocity conditions, which is tested in the context of a realistic power system.

The paper is organised as follows: In the next section, the equations describing DFIG are given, since they form the basis for the formulation of the estimation model. In Section III, the new estimation method which is developed for cases with a nonlinear unknown input is presented and thoroughly analysed. Section IV includes implementations of the proposed technique on the IEEE benchmark 68-bus, 16-machine system. Section V summarizes the contributions.

II. WIND TURBINE GENERATOR MODEL

A. Model Development

The wind turbine generator used here is considered to be an aggregate wind turbine generator model, in place of a wind

farm. The wind turbine is considered to be of Type 3, i.e. a doubly fed induction generator (DFIG). In this study, the modelling is based on the analysis performed in [16]. It has to be mentioned that the estimation model development is linked with the level of knowledge of the actual wind turbine model; thus, it is fundamental to list the equations describing the DFIG in the simulation of the actual power system, as this facilitates the estimation model specification. In this context, the full order model used in the power system simulation is comprised by the following parts:

1) *Turbine*: The presence of wind contributes to the creation of the turbine torque, which is given as follows:

$$T_t = P_{tur} / \omega_t \quad (1)$$

$$P_{tur} = 0.5 \rho \pi R_t^2 C_p(\lambda, \beta) v_w^3 \quad (2)$$

$$C_p(\lambda, \beta) = c_1 (c_2 / (\lambda + c_8 \beta) - c_2 c_9 / (\beta^3 + 1) - c_3 \beta - c_4 \beta^{c_5} - c_6) e^{-(c_7 / (\lambda + c_8 \beta) + (c_7 c_9 / (\beta^3 + 1)))} + c_{10} \lambda \quad (3)$$

$$\lambda = \omega_t R_t / v_w \quad (4)$$

where T_t , P_{tur} are the turbine torque and power, respectively, ω_t is the turbine rotor speed, ρ the air density, R_t the blade length, C_p the turbine performance coefficient, λ the tip speed ratio, β the pitch angle, v_w the wind velocity, and c_1, \dots, c_9 are the parameters of C_p curves.

2) *Drive Train*: The turbine generator mechanical system ('drive train', as referred in [17]) is represented using a simple two mass - damper- spring system modelled as follows:

$$\dot{\omega}_t = (T_t - k_t \theta_{tw} - c \dot{\theta}_{tw}) / (2H_t) \quad (5)$$

$$\dot{\omega}_r = (k_t \theta_{tw} + c \dot{\theta}_{tw} - T_e) / (2H_g) \quad (6)$$

$$\dot{\theta}_{tw} = \omega_{elB} (\omega_t - \omega_r) \quad (7)$$

where H_t , H_g are the turbine and generator inertias, respectively, ω_r is the generator rotor speed, T_e the generator electromagnetic torque, k_t the shaft stiffness, θ_{tw} the twist angle, c the damping per electrical radian, and ω_{elB} is the electrical base speed.

3) *Pitch Angle Controller & Optimum Power Point Tracking*: The WTG produces rated output for wind velocity values between the rated wind velocity and cut of wind speed (i.e. the rated operational regime). In this region the output power is limited by turning or pitching the turbine blade. The pitch angle control mechanism is modelled using the equations:

$$\dot{\Phi}_{wr} = - (1/T_{wr}) \Phi_{wr} + (1/K_{wr}) \beta_{ref} \quad (8)$$

$$\dot{\beta} = (1/T_{\beta}) (\beta_{ref} - \beta) \quad (9)$$

$$\beta_{ref} = (\omega_{r,ref} - \omega_r) K_{wr} + \Phi_{wr} K_{wr} / T_{wr} \quad (10)$$

where Φ_{wr} is the associated state variable, whereas K_{wr} , T_{wr} are the proportional gain and integral time constants of the PI controller, respectively, β_{ref} is the reference pitch angle, T_{β} is the time constant of the actuators, and $\omega_{r,ref}$ is the reference generator rotor speed. On the other hand, for wind velocity values lower than the rated one (i.e. the subrated regime), the blades are oriented to face the wind to capture maximum energy. The latter is optimised using the maximum power point tracking controller by changing the rotor speed, and, hence, the reference torque for the rotor side converter control (see

subsection II-A5). This is given below, with 'opt' subscript denoting the optimal value of the associated quantity:

$$T_{e,ref} = K_{opt} \omega_r^2 \quad (11)$$

$$K_{opt} = (0.5 \rho \pi R_t^5 C_{pmax}) / (\lambda_{opt}^3) \quad (12)$$

4) *Induction Generator*: The induction generator model used here considers that the d-axis leads the q-axis, and it does not ignore the stator transients. The equations characterising the induction generator operation are given as follows:

$$\begin{aligned} \dot{I}_{sq} &= (\omega_{elB} / L'_s) (-R_1 I_{sq} + \omega_s L'_s I_{sd} + (\omega_r E'_{sq} / \omega_s) \\ &\quad - E'_{sd} / (\omega_s T_r) - V_{sq} + K_{mrr} V_{rq}) \end{aligned} \quad (13)$$

$$\begin{aligned} \dot{I}_{sd} &= (\omega_{elB} / L'_s) (-R_1 I_{sd} - \omega_s L'_s I_{sq} + (\omega_r E'_{sd} / \omega_s) \\ &\quad + E'_{sq} / (\omega_s T_r) - V_{sd} + K_{mrr} V_{rd}) \end{aligned} \quad (14)$$

$$\begin{aligned} \dot{E}'_{sq} &= \omega_s \omega_{elB} (R_2 I_{sd} + (1 - \omega_r / \omega_s) E'_{sd} - E'_{sq} / (\omega_s T_r) \\ &\quad - K_{mrr} V_{rd}) \end{aligned} \quad (15)$$

$$\begin{aligned} \dot{E}'_{sd} &= \omega_s \omega_{elB} (-R_2 I_{sq} - (1 - \omega_r / \omega_s) E'_{sq} - E'_{sd} / (\omega_s T_r) \\ &\quad + K_{mrr} V_{rq}) \end{aligned} \quad (16)$$

$$I_{rq} = - (E'_{sd} / X_m) - K_{mrr} I_{sq} \quad (17)$$

$$I_{rd} = (E'_{sq} / X_m) - K_{mrr} I_{sd} \quad (18)$$

where

$$R_1 = R_s + K_{mrr}^2 R_r, \quad R_2 = K_{mrr}^2 R_r, \quad K_{mrr} = L_m / L_r,$$

$$L'_s = L_s - L_m^2 / L_r, \quad T_r = L_r / R_r, \quad X_m = \omega_s L_m$$

Here, I_{sq} , I_{sd} are the q & d-axis stator currents, respectively, E'_{sq} , E'_{sd} are the transient emfs due to flux in d & q-axis coils, respectively, V_{sq} , V_{sd} are the q & d-axis stator voltages, respectively, V_{rq} , V_{rd} are the q & d-axis rotor voltages, respectively, ω_s is the p.u. synchronous speed, R_s the stator resistance, R_r the rotor resistance, L_s the stator inductance, L_r the rotor inductance, and L_m is the mutual inductance.

5) *Rotor Side Converter (RSC)*: The RSC is used to energize the rotor windings with a voltage at slip frequency and carry the rotor power to the grid. The controllers of RSC can be used to regulate the generator electrical torque (by controlling active power output) and the stator reactive power output. Independent control of torque and reactive power, using the vector control approach, requires the q-axis voltage to be aligned with WTG stator voltage. However, the generator model assumes that the q-axis is aligned with the slack bus voltage defined in the power flow; thus, these voltages and currents must be transferred to a new axis aligned to the WTG terminal bus voltage. A phase-locked loop (PLL) is used to find the angle of rotation required to bring voltage and current vectors to the new axis. The RSC uses two cascaded PI controllers in both q & d axes. The relevant equations are:

$$I'_{rq} + j I'_{rd} = (I_{rq} + j I_{rd}) e^{-j\theta_p} \quad (19)$$

$$\dot{\Phi}_{Te} = K_{i,Te} (T_{e,ref} - T_e) \quad (20)$$

$$\dot{\Phi}_{iq} = K_{i,iq} [\Phi_{Te} + K_{p,Te} (T_{e,ref} - T_e) - I'_{rq}] \quad (21)$$

$$V'_{rq} = \Phi_{iq} + K_{p,iq} [\Phi_{Te} + K_{p,Te} (T_{e,ref} - T_e) - I'_{rq}] \quad (22)$$

$$\dot{\Phi}_{Qs} = K_{i,Qs} (Q_{s,ref} - Q_s) \quad (23)$$

$$\dot{\Phi}_{id} = K_{i,id} [\Phi_{Qs} + K_{p,Qs} (Q_{s,ref} - Q_s) - I'_{rd}] \quad (24)$$

$$V'_{rd} = \Phi_{id} + K_{p,id} [\Phi_{Qs} + K_{p,Qs} (Q_{s,ref} - Q_s) - I'_{rd}] \quad (25)$$

$$V_{rq} + jV_{rd} = (V'_{rq} + jV'_{rd}) e^{j\theta_p} \quad (26)$$

$$T_e = L_m (I_{sq}I_{rd} - I_{sd}I_{rq}) \quad (27)$$

$$Q_s = V_{sd}I_{sq} - V_{sq}I_{sd} \quad (28)$$

where I'_{rq} , I'_{rd} are the q & d-axis rotor currents, respectively, θ_p is the phasor argument determined by the PLL (see below), Φ_{Te} , Φ_{iq} are the state variables related to electromagnetic torque PI control, with $K_{p,Te}$, $K_{i,Te}$, $K_{p,iq}$, $K_{i,iq}$ its associated constants, whereas, Φ_{Qs} , Φ_{id} are the state variables related to reactive power PI control, with $K_{p,Qs}$, $K_{i,Qs}$, $K_{p,id}$, $K_{i,id}$ its associated constants, $T_{e,ref}$ is related to maximum power point tracking, and $Q_{s,ref}$ is the reference value for Q_s , which in this case is equal to the value obtained from the power flow for the wind turbine's terminal bus.

6) *Phase Locked Loop (PLL)*: The PLL is described by the equations below [18], [19]:

$$\dot{x}_{1,p} = c_{1,p} [Im((V_{sq} + jV_{sd}) e^{-j\theta_p}) - x_{1,p}] \quad (29)$$

$$\dot{x}_{2,p} = c_{2,p} x_{1,p} \quad (30)$$

$$\dot{\theta}_p = c_{3,p} x_{1,p} + x_{2,p} \quad (31)$$

where $x_{1,p}$, $x_{2,p}$ are the rest of the state variables associated with the PLL operation, and $c_{i,p}$, $i = 1, 2, 3$ are parameters.

7) *Grid Side Converter (GSC) & Filter*: The GSC consists of a converter and a filter to remove switching harmonics. Here, an LCL filter is assumed [20]. The switching frequency dynamics of the GSC are not included in the model, and the GSC is represented by two converter controller models, along with the capacitor dynamics (DC link - see subsection II-A8). Vector control approach is used for the GSC, which regulates the DC capacitor voltage (ensuring that rotor power is seamlessly transferred) and reactive power transfer through the GSC (zero reactive power transfer through GSC is assumed) [21]. The equations are listed below:

$$\dot{I}_{iq} = \frac{w_{elB}}{L_i} [V_{iq} - V_{cq} - (R_i + R_c) I_{iq} + w_s L_i I_{id} + R_c I_{gq}] \quad (32)$$

$$\dot{I}_{id} = \frac{w_{elB}}{L_i} [V_{id} - V_{cd} - (R_i + R_c) I_{id} - w_s L_i I_{iq} + R_c I_{gd}] \quad (33)$$

$$\dot{I}_{gq} = \frac{w_{elB}}{L_g} [V_{cq} - V_{sq} - (R_g + R_c) I_{gq} + w_s L_g I_{gd} + R_c I_{iq}] \quad (34)$$

$$\dot{I}_{gd} = \frac{w_{elB}}{L_g} [V_{cd} - V_{sd} - (R_g + R_c) I_{gd} - w_s L_g I_{gq} + R_c I_{id}] \quad (35)$$

$$\dot{V}_{cq} = (w_{elB}/C_f)(I_{iq} - I_{gq} + w_s C_f V_{cd}) \quad (36)$$

$$\dot{V}_{cd} = (w_{elB}/C_f)(I_{id} - I_{gd} - w_s C_f V_{cq}) \quad (37)$$

$$I'_{gq} + jI'_{gd} = (I_{gq} + jI_{gd}) e^{-j\theta_p} \quad (38)$$

$$\dot{\Phi}_{igq} = K_{i,igq} (V_{dcref} - V_{dc}) \quad (39)$$

$$\dot{\Phi}_{viq} = K_{i,viq} [\Phi_{igq} + K_{p,igq} (V_{dcref} - V_{dc}) - I'_{gq}] \quad (40)$$

$$V'_{iq} = \Phi_{viq} + K_{p,viq} [\Phi_{igq} + K_{p,igq} (V_{dcref} - V_{dc}) - I'_{gq}] \quad (41)$$

$$\dot{\Phi}_{igd} = K_{i,igd} (Q_{r,ref} - Q_r) \quad (42)$$

$$\dot{\Phi}_{vid} = K_{i,vid} [\Phi_{igd} + K_{p,igd} (Q_{r,ref} - Q_r) - I'_{gd}] \quad (43)$$

$$V'_{id} = \Phi_{vid} + K_{p,vid} [\Phi_{igd} + K_{p,igd} (Q_{r,ref} - Q_r) - I'_{gd}] \quad (44)$$

$$V_{iq} + jV_{id} = (V'_{iq} + jV'_{id}) e^{j\theta_p} \quad (45)$$

$$Q_r = V_{rd}I_{rq} - V_{rq}I_{rd} \quad (46)$$

where I_{iq} , I_{id} are the q & d-axis currents through the inverter-side filter inductor, respectively, I_{gq} , I_{gd} the q & d-axis currents through the grid-side filter inductor, respectively, V_{cq} , V_{cd} the q & d-axis back-to-back capacitor voltages, respectively, V_{iq} , V_{id} the q & d-axis voltages at the inverter terminal, respectively, R_i is the inverter-side resistance, R_g the grid-side resistance, R_c the damping resistance, L_i the inverter-side inductance, L_g the grid-side inductance, C_f the filter capacitor, Φ_{igq} , Φ_{viq} are the state variables related to the DC-link capacitor voltage PI control, with $K_{p,igq}$, $K_{i,igq}$, $K_{p,viq}$, $K_{i,viq}$ its associated constants, Φ_{igd} , Φ_{vid} are the state variables related to reactive power PI control for the GSC to the terminal bus, with $K_{p,igd}$, $K_{i,igd}$, $K_{p,vid}$, $K_{i,vid}$ its associated constants, V_{dc} is the DC-link capacitor voltage, Q_r is the generator rotor reactive power, and V_{dcref} , $Q_{r,ref}$ are the reference values for V_{dc} and Q_r , respectively, which are set to 1 p.u. and 0, respectively.

8) *DC Link*: The equations are given below [21]:

$$\dot{V}_{dc} = (C_{dc}/V_{dc})(P_r - P_{GSC}) \quad (47)$$

$$P_r = V_{rq}I_{rq} + V_{rd}I_{rd} \quad (48)$$

$$P_{GSC} = V_{iq}I_{iq} + V_{id}I_{id} \quad (49)$$

where C_{dc} is the DC-link capacitor, P_r the generator rotor active power, and P_{GSC} the GSC output active power.

B. Estimation model specification

Equations (1)-(49) comprise the full-order wind turbine model used as part of the power system model under study. However, the estimation model, which is utilized in the context of the DSE procedure, is a reduced version of the full-order one, for observability and numerical integration reasons. Thus, the estimation model includes the discrete form of the differential equations (15), (16), (20), (21), (23), (24), (39), (40), (42), (43), (47). Moreover, (13), (14), (32)-(37) are set to zero (thus considered as algebraic equations), whereas $V_{sq} = V_t$ and $V_{sd} = 0$, where V_t is the terminal bus voltage, so as to avoid the need to include the PLL equations ((29)-(31)) in the context of the estimation model, to reduce complexity. Equations (1)-(10) lie outside the estimation model boundary. Fig. 1 shows how the estimation model used for the estimation purposes is related to the full order model, which is utilized for the simulation of the real system. This model includes one unknown input, the rotor speed (w_r), which is affected by the unknown wind velocity, which is the basic realistic scenario of this study. The discretization is based on the principle $\dot{x} \approx (x_k - x_{k-1})/T_0$, where T_0 is the simulation time step. The simulation time step is associated with the Phasor Measurement Unit (PMU) reporting rate, and this is the reason behind the use of a reduced order model; several dynamic equations are characterised by very low time constants compared to the simulation time step, hence it is preferable for them to be regarded as algebraic, to ensure that

the estimation procedure does not diverge. Therefore, the state vector has the form below:

$$x = [E'_{sq} \ E'_{sd} \ \Phi_{Te} \ \Phi_{iq} \ \Phi_{Qs} \ \Phi_{id} \ V_{dc} \ \Phi_{igq} \ \Phi_{viq} \ \Phi_{igd} \ \Phi_{vid}]^T \quad (50)$$

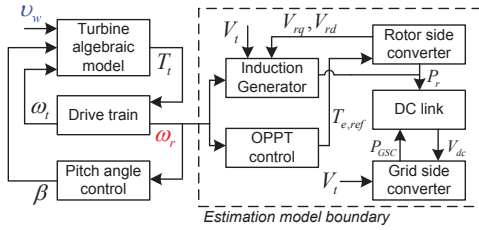


Fig. 1. The estimation model boundary with respect to the full order model

The noise-free part of the output measurement equations of the estimation model at every time instant k are the following:

$$I_{tk} = \sqrt{(I_{sqk} + I_{gqk})^2 + (I_{sdk} + I_{gdk})^2} \quad (51)$$

$$\phi_k = \arctan\left(\frac{I_{sdk} + I_{gdk}}{I_{sqk} + I_{gqk}}\right) \quad (52)$$

$$P_{tk} = E'_{sqk} I_{sqk} + E'_{sdk} I_{sdk} + V_{iqk} I_{iqk} + V_{idk} I_{idk} - R_s (I_{sqk}^2 + I_{sdk}^2) \quad (53)$$

$$Q_{tk} = E'_{sdk} I_{sqk} - E'_{sqk} I_{sdk} - V_{sqk} I_{gdk} + V_{sdk} I_{gqk} - w_s L'_s (I_{sqk}^2 + I_{sdk}^2) \quad (54)$$

where I_t , ϕ , P_t , Q_t are the terminal bus current magnitude, argument, active and reactive power, respectively.

III. DYNAMIC STATE ESTIMATION WITH A NONLINEAR UNKNOWN INPUT

A. Problem formulation

The power system state space model, including the wind turbine generator, is given by the following set of discrete nonlinear differential-algebraic equations (DAEs):

$$\begin{aligned} x_k &= f(x_{k-1}, u_{k-1}, d_{k-1}, w_{k-1}) \\ y_k &= h(x_k, u_k) + v_k \end{aligned} \quad (55)$$

where x and w are n -dimensional vectors of state variables and process noise, respectively, u is a r -dimensional vector of system (known) inputs, d is a scalar denoting the unknown input of the estimation model, y and v are m -dimensional vectors of measurements and measurement noise, respectively, whereas, f and h refer to the system dynamic state and output measurement equations, respectively. The process and output measurement noise vectors are considered to be Gaussian, zero-mean, white and uncorrelated to each other, with Q_k , R_k being the process and output measurement noise covariances at time instant k , respectively.

Given the wind turbine model used here, it is clear that the unknown input (w_r) has a nonlinear relationship with the states, therefore the procedure outlined in [8] is not suitable for this context, since it addresses cases of additive unknown inputs. The employment of a sigma-point based approach like the Cubature Kalman filter (CKF) avoids the calculation of derivatives, hence, this derivative-free principle is kept in the

context of the unknown input estimation. For this reason, all output equations are expressed as power series of the unknown input, then, an objective function is defined, and the unknown input is computed as a solution of an eigenvalue problem for an equivalent matrix.

The algorithm is described in the sections below:

B. Biased State Estimation

Similarly to [8], the dynamic state estimation procedure starts with the biased state estimation part, given the lack of knowledge of the unknown input's value. The state prediction is conducted as follows:

1) *Sigma point generation*: CKF relies on the creation of a family of points, which capture several statistical properties of random variables, and, here, it is the mean and the covariance of x . CKF is based on the following collection of sigma points:

$$\begin{aligned} \chi_{k-1}^{(l)} &= [\hat{x}_{k-1}^{u+} + \tilde{x}^{(l)}], \quad l = 1, 2, \dots, 2n \\ \tilde{x}^{(l)} &= \left(\sqrt{nP_{k-1}^{u+}} \right)_l, \quad l = 1, 2, \dots, n \\ \tilde{x}^{(n+l)} &= - \left(\sqrt{nP_{k-1}^{u+}} \right)_l, \quad l = 1, 2, \dots, n \end{aligned} \quad (56)$$

where \hat{x}_{k-1}^{u+} and P_{k-1}^{u+} are the unbiased dynamic state estimate and the unbiased a posteriori state estimate error covariance of the previous time step, respectively. Additionally, $\left(\sqrt{nP_{k-1}^{u+}} \right)_l$ is the l th column of the lower triangular matrix resulting from the Cholesky decomposition: $nP_{k-1}^{u+} = \sqrt{nP_{k-1}^{u+}} \sqrt{nP_{k-1}^{u+}}^T$.

2) *Biased state prediction*: Here, the sigma points are instantiated through the process model, and the state prediction is obtained. The state prediction is biased, since the unknown inputs are not considered in the calculation procedure:

$$\chi_k^{b(l)} = f\left(\chi_{k-1}^{(l)}, u_{k-1}\right) \quad (57)$$

where

$$\begin{aligned} \chi_{k-1}^{(l)} &= [\hat{x}_{k-1}^{u+} + \tilde{x}^{(l)}], \quad l = 1, 2, \dots, 2n \\ \tilde{x}^{(l)} &= \left(\sqrt{nP_{k-1}^{u+}} \right)_l, \quad l = 1, 2, \dots, n \\ \tilde{x}^{(n+l)} &= - \left(\sqrt{nP_{k-1}^{u+}} \right)_l, \quad l = 1, 2, \dots, n \end{aligned} \quad (58)$$

$$\hat{x}_k^b = \frac{1}{2n} \sum_{l=1}^{2n} \chi_k^{b(l)} \quad (59)$$

In the above equations, χ_k^b are the biased predicted sigma points, and \hat{x}_k^b is the biased state prediction.

3) *Biased measurement prediction*: Here, the sigma points are instantiated through the output measurement equations, so as to obtain the biased output measurement prediction (\hat{y}_k^b):

$$\gamma_k^{b(l)} = h\left(\chi_k^{b(l)}, u_k\right), \quad \hat{y}_k^b = \frac{1}{2n} \sum_{l=1}^{2n} \gamma_k^{b(l)} \quad (60)$$

where γ_k^b are the biased predicted measurement sigma points.

C. Unknown Input Estimation

The high nonlinearity characterising the wind turbine generator estimation model does not facilitate the utilization of the CKF-UI algorithm developed in [8], since, in that case, the unknown inputs were additive, and the unknown estimation procedure was based on the statistical linearisation of the nonlinear output measurement functions. However, here, the unknown input is nonlinear with respect to the states, and, given the nonlinear output measurement functions, the statistical linearisation poorly captures the unknown input's effect on the measurement equations. Thus, another unknown input estimation procedure is needed, which has to keep the nonlinear nature of the measurement functions. Given that the employment of CKF does not require the calculation of any derivatives, the new approach is preferred to be derivative-free. For this purpose, the following procedure is employed: First, the output measurement functions are reformulated as power series of the unknown input (w_r):

$$I_t = I_t^{ba} + I_{tlin}w_r + I_{tsqa}w_r^2 + v_I \quad (61)$$

$$\begin{aligned} \phi = & \phi_m + K_{\phi 0} + K_{\phi 1}w_r + K_{\phi 2}w_r^2 + K_{\phi 3}w_r^3 \\ & + K_{\phi 4}w_r^4 + v_\phi \end{aligned} \quad (62)$$

$$P_t = P_t^b + P_{tlin}w_r + P_{tsq}w_r^2 + v_P \quad (63)$$

$$Q_t = Q_t^b + Q_{tlin}w_r + Q_{tsq}w_r^2 + v_Q \quad (64)$$

where v denotes measurement noise for each quantity.

The details of the derivation of these power series, along with the definition of constants, are given in Appendix A. Given this form of the measurement equations, the following objective function is sought to be minimized:

$$R_{obj}^2 = v_I^2 + v_\phi^2 + v_P^2 + v_Q^2 \quad (65)$$

This means that the solution sought should make the first derivative of the objective function equal to zero, therefore the unknown input is one of the solutions of the following equation:

$$C_0 + C_1w_r + C_2w_r^2 + C_3w_r^3 + C_4w_r^4 + C_5w_r^5 + C_6w_r^6 + C_7w_r^7 = 0 \quad (66)$$

where

$$\begin{aligned} C_0 = & -I_{tlin}(I_t - I_t^{ba}) - K_{\phi 1}(\phi - \phi_m - K_{\phi 0}) \\ & - P_{tlin}(P_t - P_t^b) - Q_{tlin}(Q_t - Q_t^b) \end{aligned} \quad (67)$$

$$\begin{aligned} C_1 = & -2I_{tsqa}(I_t - I_t^{ba}) + I_{tlin}^2 - 2K_{\phi 2}(\phi - \phi_m - K_{\phi 0}) \\ & + K_{\phi 1}^2 - 2P_{tsq}(P_t - P_t^b) + P_{tlin}^2 \\ & - 2Q_{tsq}(Q_t - Q_t^b) + Q_{tlin}^2 \end{aligned} \quad (68)$$

$$\begin{aligned} C_2 = & 3I_{tlin}I_{tsqa} - 3K_{\phi 3}(\phi - \phi_m - K_{\phi 0}) + 3K_{\phi 1}K_{\phi 2} \\ & + 3P_{tlin}P_{tsq} + 3Q_{tlin}Q_{tsq} \end{aligned} \quad (69)$$

$$\begin{aligned} C_3 = & 2I_{tsqa}^2 - 4K_{\phi 4}(\phi - \phi_m - K_{\phi 0}) + 4K_{\phi 1}K_{\phi 3} \\ & + 2K_{\phi 2}^2 + 2P_{tsq}^2 + 2Q_{tsq}^2 \end{aligned} \quad (70)$$

$$C_4 = 5K_{\phi 1}K_{\phi 4} + 5K_{\phi 2}K_{\phi 3} \quad (71)$$

$$C_5 = 6K_{\phi 2}K_{\phi 4} + 3K_{\phi 3}^2 \quad (72)$$

$$C_6 = 7K_{\phi 3}K_{\phi 4} \quad (73)$$

$$C_7 = 4K_{\phi 4}^2 \quad (74)$$

This formulation allows the computation of the unknown input in a straightforward manner, since the solutions of this equation are the eigenvalues of the following matrix [22]:

$$A = \begin{bmatrix} 0 & 1 & \cdots & 0 \\ \vdots & \vdots & \ddots & \vdots \\ 0 & 0 & \cdots & 1 \\ -\frac{C_0}{C_7} & -\frac{C_1}{C_7} & \cdots & -\frac{C_6}{C_7} \end{bmatrix} \quad (75)$$

The preferred solution is the real eigenvalue for which the objective function (65) has the minimum value.

D. Unbiased State Estimation

Following the unknown input estimation, the standard CKF procedure is followed, since the previously unknown input is now known. The CKF algorithm is given as follows:

1) Unbiased (a priori) state prediction:

$$\chi_k^{u(l)} = f(\chi_{k-1}^{(l)}, u_{k-1}, \hat{d}_{k-1}), \quad \hat{x}_k^{u-} = \frac{1}{2n} \sum_{l=1}^{2n} \chi_k^{u(l)} \quad (76)$$

where χ_k^u are the unbiased state prediction sigma points, \hat{d}_{k-1} is the unknown input estimate for the time instant $k-1$, and \hat{x}_k^{u-} is the unbiased a priori state estimate.

2) Unbiased a priori state error covariance calculation:

$$P_k^{u-} = \frac{1}{2n} \sum_{l=1}^{2n} (\chi_k^{u(l)} - \hat{x}_k^{u-}) (\chi_k^{u(l)} - \hat{x}_k^{u-})^T \quad (77)$$

where P_k^{u-} is the unbiased a priori state estimate error covariance.

3) Unbiased measurement prediction:

$$\gamma_k^{u(l)} = h(\chi_k^{u(l)}, u_k), \quad \hat{y}_k^u = \frac{1}{2n} \sum_{l=1}^{2n} \gamma_k^{u(l)} \quad (78)$$

where γ_k^u are the unbiased measurement prediction sigma points, and \hat{y}_k^u is the unbiased measurement prediction.

4) Unbiased measurement prediction error covariance estimation:

$$P_{yk}^u = \frac{1}{2n} \sum_{l=1}^{2n} (\gamma_k^{u(l)} - \hat{y}_k^u) (\gamma_k^{u(l)} - \hat{y}_k^u)^T + R_k \quad (79)$$

where P_{yk}^u is the unbiased measurement prediction error covariance.

5) Calculation of the unbiased cross-covariance between the states and the predicted measurements:

$$P_{xyk}^u = \frac{1}{2n} \sum_{l=1}^{2n} (\chi_k^{u(l)} - \hat{x}_k^{u-}) (\gamma_k^{u(l)} - \hat{y}_k^u)^T \quad (80)$$

where P_{xyk}^u is the unbiased cross-covariance between \hat{x}_k^{u-} , \hat{y}_k^u .

6) *Measurement update of the state estimate (or a posteriori state estimate):*

$$K_k = P_{xyk}^u (P_{yk}^u)^{-1} \quad (81)$$

$$\hat{x}_k^+ = \hat{x}_k^- + K_k (y_k - \hat{y}_k^u) \quad (82)$$

$$P_k^+ = P_k^- - K_k P_{yk}^u K_k^T \quad (83)$$

where K_k is the Kalman gain matrix.

The steps (56)-(83) constitute the proposed CKF based algorithm for dynamic state and unknown nonlinear input estimation for wind turbine generators, used here. All these calculations are repeated at every time step.

IV. CASE STUDIES

The suggested DSE scheme has been applied to the IEEE benchmark 68-bus, 16-machine NETS-NYPS system [23]. The details of this system can be found in [24], and it is depicted in Fig. 2. The proposed estimation technique has been tested with respect to 4 case studies, to address cases of different wind turbine operating regions, various wind trajectory patterns as well as different grid operating conditions. In all case studies, the measurements are obtained at the wind turbine's terminal bus. For all measurements, along with the measured input (i.e. V), Gaussian noise of standard deviation of 10^{-3} has been considered, which lies within the measurement noise limits dictated by the IEEE Standard C37.118.1-2011, which sets as maximum 1% total vector error (TVE) for PMU measurements, blending together three possible sources of error for each phasor: phasor magnitude, angle and time synchronisation [25]. The simulation time step is 0.83 ms, and, given the absence of commercial PMUs with such a high reporting rate (this would correspond to 1200 Hz), pseudo-measurements are employed by performing measurement interpolation between two successive PMU measurements, in a similar way as conducted in [26]. Therefore, assuming IEEE Standards-compliant PMUs with reporting rate of 120 Hz, this corresponds to 10 measurements per 8.3 ms. Such low simulation time step is driven by the low time constants of the estimation model differential equations. Power system modelling is MATLAB/Simulink based, and the simulation lasts for 5 seconds. The following case studies have been considered:

1) *Sub-rated region, sinusoidally varying wind velocity:*

The synchronous machine at bus 1 has been replaced by a wind turbine model which simulates a wind farm of equivalent capacity, comprised of 100 wind turbines. The wind turbine operates in the sub-rated operating region, with the wind speed being equal to 11.96 m/s in the beginning of the simulation, corresponding to active power output of 2.5 MW for each wind turbine. The full order model has been used in the context of the simulation of the system model. The details of the wind turbine parameters can be found in Appendix B. The wind velocity pattern considered is sinusoidal, and Gaussian noise of 0.5 (m/s)^2 variance has been added as well, to account for turbulence. The wind velocity trajectory for this case study is illustrated in Fig. 3. The dynamic state estimation results are shown in Figs. 4 and 5, whereas the unknown input estimation results are depicted in Fig. 6. The estimation

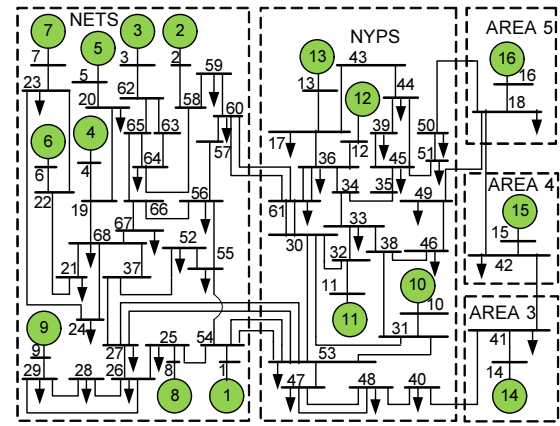


Fig. 2. NETS-NYPS 68-bus, 16-machine system

procedure proves to be successful against highly varying wind velocity conditions, with turbulence being present.

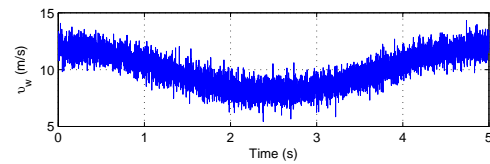


Fig. 3. Wind velocity trajectory for case studies 1 and 4.

2) *Sub-rated region, oscillating wind velocity:* The same system setup has been followed as in the previous case study, but a different wind velocity pattern has been regarded: Here, small variations are considered around the value of 11.96 m/s, and these variations have been generated by the addition of Gaussian noise of 1 m/s standard deviation, as shown in Fig. 7. The dynamic state estimation results are depicted in Figs. 8 and 9, whereas the unknown input estimation results are illustrated in Fig. 10. The results show high accuracy with respect to slightly varying wind velocity conditions.

3) *Rated region, sinusoidally varying wind velocity:* The wind turbine considered operates in the rated region, with the wind speed being equal to 19 m/s in the beginning of the simulation. Thus, to match the capacity of the synchronous generator which is replaced at bus 1, the wind turbine model is assumed to simulate a wind farm of equivalent capacity, comprised of 50 wind turbines, corresponding to active power output of 5 MW each, operating in the rated region. In this case study, the wind velocity pattern is sinusoidal, with Gaussian noise of 0.2 (m/s)^2 variance added, as depicted in Fig. 11. The dynamic state estimation results are illustrated in Figs. 12 and 13, and the unknown input estimation results are shown in Fig. 10. It can be clearly noticed that the estimation algorithm is also successful in the rated operating region of the wind turbine, accurately tracking its response under significantly varying wind velocity conditions.

4) *Weak grid consideration:* Given that the system used in the previous case studies is strong, the estimation procedure has been tested on a Thevenin equivalent of a weak grid [27], with Short-circuit Ratio (SCR) equal to 2, which has been determined in accordance with the information provided by

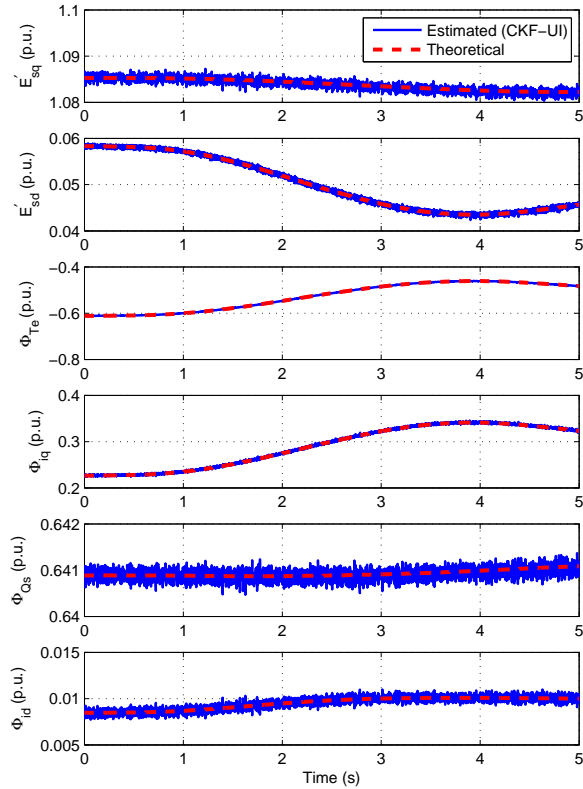


Fig. 4. Case Study 1: Dynamic state estimation results for E'_{sq} , E'_{sd} , Φ_{Te} , Φ_{iq} , Φ_{Qs} , and Φ_{id} .

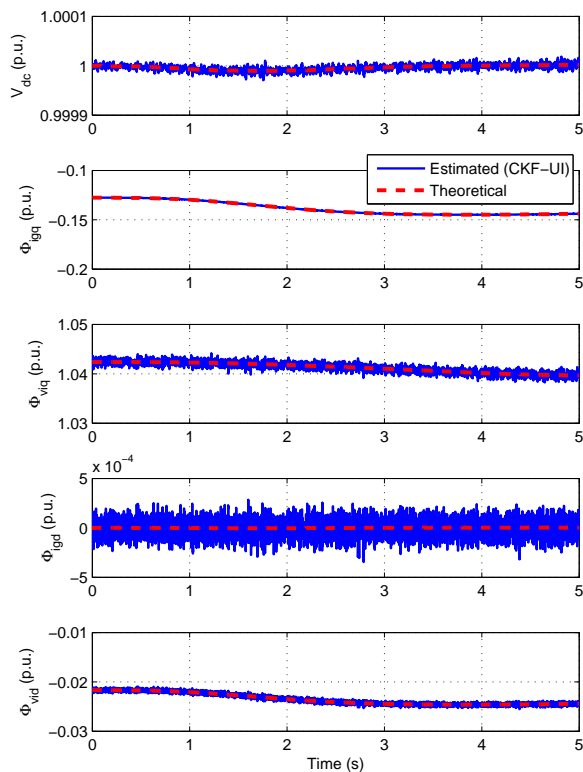


Fig. 5. Case Study 1: Dynamic state estimation results for V_{dc} , Φ_{igq} , Φ_{viq} , Φ_{igd} , and Φ_{vid} .

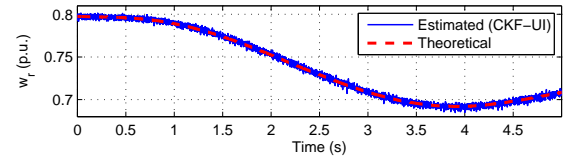


Fig. 6. Case Study 1: Unknown input estimation results for the wind turbine estimation model.

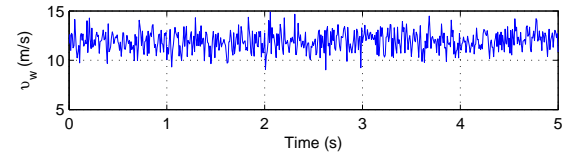


Fig. 7. Wind velocity trajectory for case study 2.

the North American Electric Reliability Corporation (NERC) [28]. Given this SCR value, the voltage source of the Thevenin equivalent is, without loss of generality, $0.88\angle -26.23^\circ$ p.u. and the Thevenin reactance is 0.546 p.u.. The wind turbine characteristics are the same as in case study 1. The same applies for the wind velocity assumed for the case. It is noted that the determination of the Thevenin equivalent parameters has been driven by the intention to match the voltage value at the wind turbine's terminal bus to the one of bus 1 of the 68-bus, 16-machine system, where the wind turbine is connected in the previous case studies, so as to perform a fair comparison, especially with respect to the first case study, where the wind velocity pattern is the same. Figs. 15 and 16 illustrate the dynamic state estimation results, whereas Fig. 17 depict the unknown input estimation outcomes. It can be observed that, although the terminal voltage is sensitive to changes in the system, the estimation technique is able to track the wind turbine's dynamics.

V. CONCLUSIONS

A derivative-free Kalman filtering based dynamic state estimation technique has been developed, to tackle cases when there is a nonlinear unknown input in the estimation models. This method has been developed to be implemented in the context of a doubly-fed induction generator based wind generator model, under the assumption of unknown or uncertain wind velocity. This algorithm is employed, given that the output measurement equations are formulated as power series. The proposed technique has been successfully applied to the IEEE benchmark 68-bus, 16-machine NETS-NYPS system, as well as to an equivalent system representing a weak grid, verifying that the estimation model's states can be accurately estimated, under uncertain wind velocity conditions. It has to be highlighted that this result is significant, since operators are given the opportunity to gain knowledge of the operational status of generators which are driven by stochastic sources. This methodology can be proven very beneficial for power system monitoring, in the context of modern power networks, which are characterised by components of highly nonlinear nature and occasionally unpredictable behaviour.

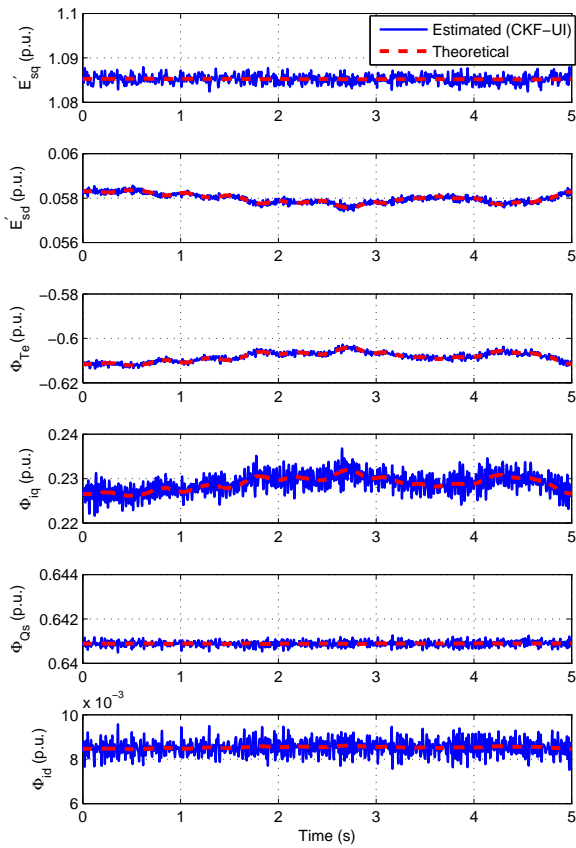


Fig. 8. Case Study 2: Dynamic state estimation results for E'_{sq} , E'_{sd} , Φ_{Te} , Φ_{iq} , Φ_{Qs} , and Φ_{id} .

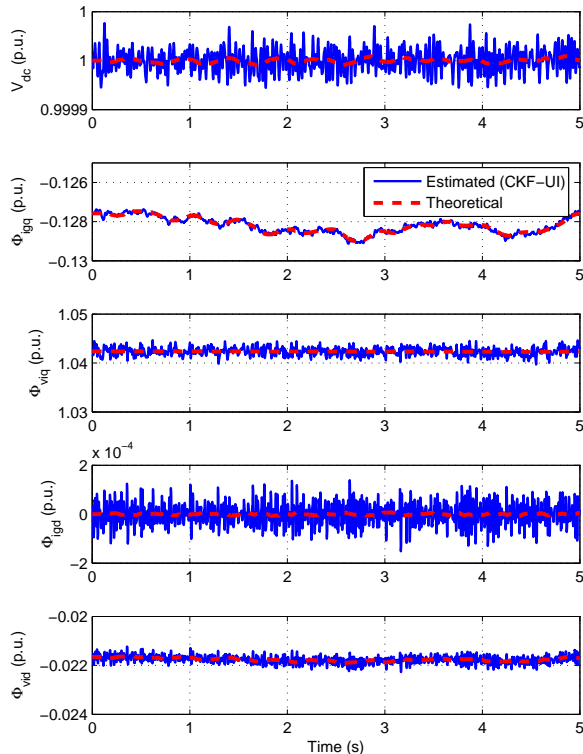


Fig. 9. Case Study 2: Dynamic state estimation results for V_{dc} , Φ_{igq} , Φ_{viq} , Φ_{igd} , and Φ_{vid} .

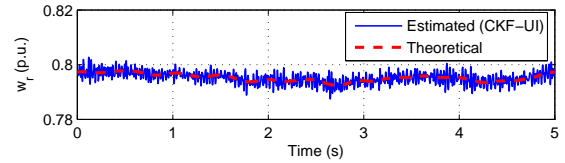


Fig. 10. Case Study 2: Unknown input estimation results for the wind turbine estimation model.

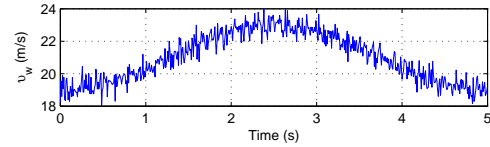


Fig. 11. Wind velocity trajectory for case study 3.

APPENDIX A

OUTPUT MEASUREMENT FUNCTIONS REFORMULATION

The concept is to calculate the value of w_r based on the measurements obtained, as well as the biased output measurement predictions made, given the fact that w_r is unknown. For instance, when making the biased measurement prediction (60), regarding the active and reactive power output P_{tk} , Q_{tk} , according to (53), (54), they can be formulated as a power series of the unknown variable $w_{r(k-1)}$, given that E'_{sqk} , E'_{sdk} , I_{sqk} , I_{sdk} are functions of $w_{r(k-1)}$, according to the state equations of the estimation model. Therefore, at time instant k , the parameters of (53), (54) are given as follows (with the b superscript referring to biased predictions - (59)):

$$P_t^b = E'_{sqk} I_{sqk}^b + E'_{sdk} I_{sdk}^b + V_{iqk} I_{iqk} + V_{idk} I_{idk} - R_s (I_{sqk}^{b2} + I_{sdk}^{b2}) \quad (84)$$

$$P_{tlin} = K_{Iq} E'_{sqk} + K_{Eq} I_{sqk}^b + K_{Id} E'_{sdk} + K_{Ed} I_{sdk}^b - 2R_s (I_{sqk}^b K_{Iq} + I_{sdk}^b K_{Id}) \quad (85)$$

$$P_{tsq} = K_{Eq} K_{Iq} + K_{Ed} K_{Id} - R_s (K_{Iq}^2 + K_{Id}^2) \quad (86)$$

where

$$K_{Iq} = \frac{w_{elB} T_0}{R_s^2 + w_s^2 L_s^2} (-R_s E'_{sd(k-1)} + w_s L_s' E'_{sq(k-1)}) \quad (87)$$

$$K_{Id} = \frac{w_{elB} T_0}{R_s^2 + w_s^2 L_s^2} (R_s E'_{sq(k-1)} + w_s L_s' E'_{sd(k-1)}) \quad (88)$$

$$Q_t^b = E'_{sdk} I_{sqk}^b - E'_{sqk} I_{sdk}^b - V_{sqk} I_{gdk} + V_{sdk} I_{gqk} - w_s L_s' (I_{sqk}^{b2} + I_{sdk}^{b2}) \quad (89)$$

$$Q_{tlin} = K_{Iq} E'_{sdk} + K_{Ed} I_{sqk}^b - K_{Id} E'_{sqk} - K_{Eq} I_{sdk}^b - 2w_s L_s' (I_{sqk}^b K_{Iq} + I_{sdk}^b K_{Id}) \quad (90)$$

$$Q_{tsq} = K_{Ed} K_{Iq} - K_{Eq} K_{Id} - w_s L_s' (K_{Iq}^2 + K_{Id}^2) \quad (91)$$

The cases concerning I_t and ϕ require special attention, since, unlike P_t , and Q_t , they cannot straightaway be expressed as power series. For this purpose, the power series formulae are employed for arctan, square root, and rational

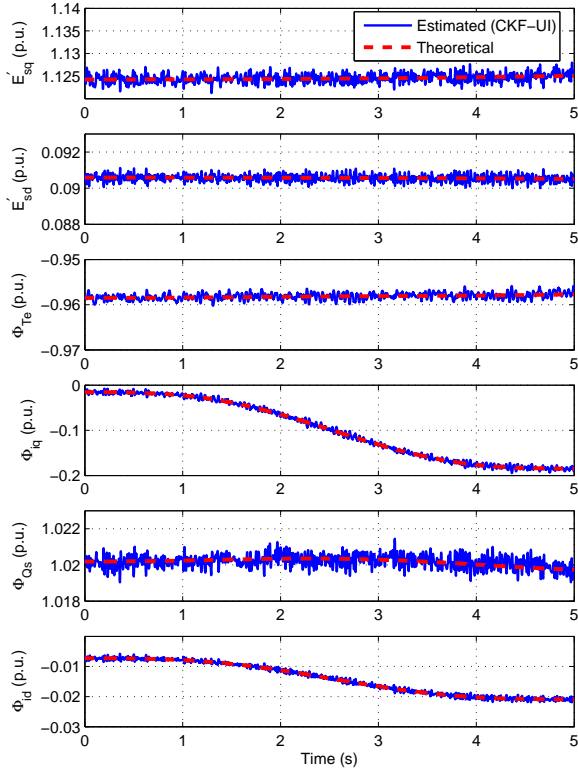


Fig. 12. Case Study 3: Dynamic state estimation results for E'_{sq} , E'_{sd} , Φ_{Te} , Φ_{iq} , Φ_{Qs} , and Φ_{id} .

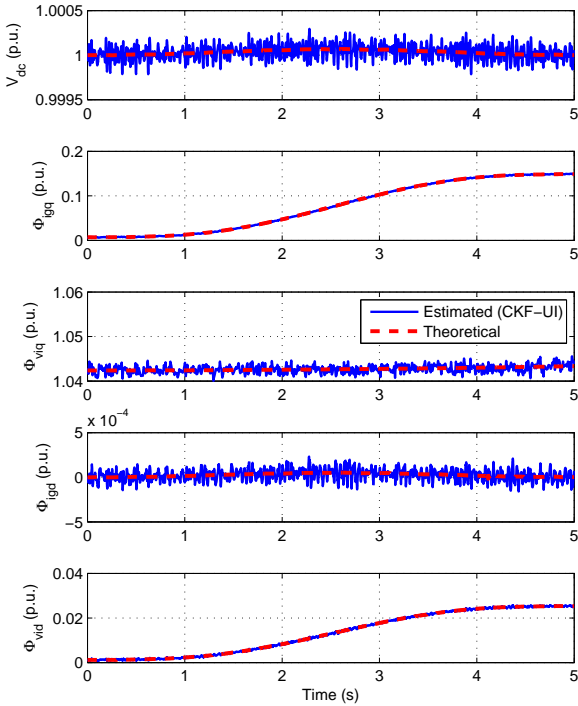


Fig. 13. Case Study 3: Dynamic state estimation results for V_{dc} , Φ_{igq} , Φ_{viq} , Φ_{igd} , and Φ_{vid} .

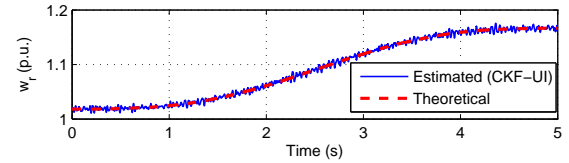


Fig. 14. Case Study 3: Unknown input estimation results for the wind turbine estimation model.

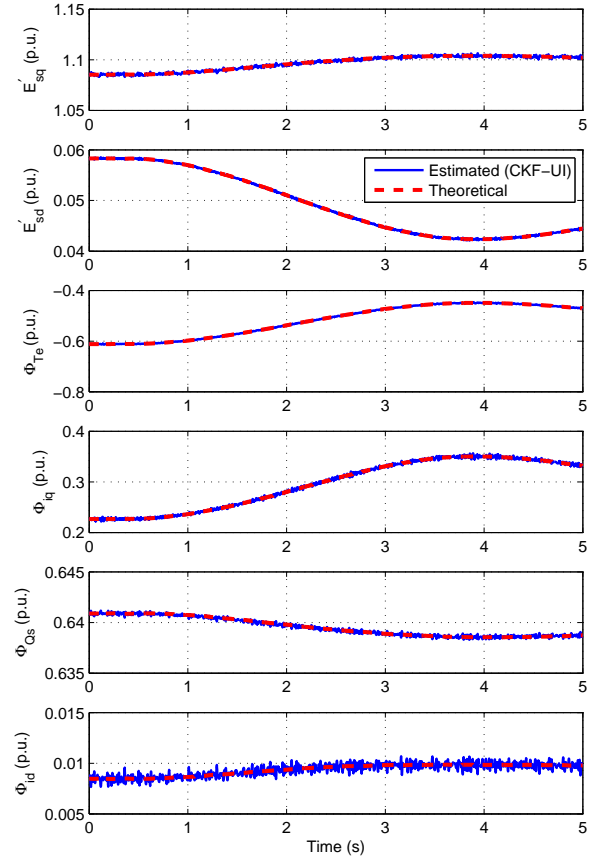


Fig. 15. Case Study 4: Dynamic state estimation results for E'_{sq} , E'_{sd} , Φ_{Te} , Φ_{iq} , Φ_{Qs} , and Φ_{id} .

functions. Regarding I_t , since I_{sqk} and I_{sdk} are functions of $w_r(k-1)$, (51) takes the following form:

$$I_t = \sqrt{I_{tb}^2 + I_{lin}w_r(k-1) + I_{sq}w_r^2(k-1)} \quad (92)$$

where

$$I_{tb}^2 = (I_{sqk}^b + I_{gqk})^2 + (I_{sdk}^b + I_{gdk})^2 \quad (93)$$

$$I_{lin} = 2 [K_{Iq} (I_{sqk}^b + I_{gqk}) + K_{Id} (I_{sdk}^b + I_{gdk})] \quad (94)$$

$$I_{sq} = K_{Iq}^2 + K_{Id}^2 \quad (95)$$

The purpose is to transform (92) in the form of $\sqrt{(\cdot)}\sqrt{1 + \kappa}$, with κ almost 0, so as to be able to use the first order term only of the standard power series formula for $\sqrt{1 + \kappa}$. Thus, if (92) is expressed as $\sqrt{I_{tb}^2 + \zeta}$, with $\zeta = I_{lin}w_r(k-1) + I_{sq}w_r^2(k-1)$, then it can be given as

$$\sqrt{I_{tb}^2 + \zeta} = \sqrt{I_{tb}^2 + \xi} \sqrt{1 + \frac{\zeta - \xi}{I_{tb}^2 + \xi}}$$

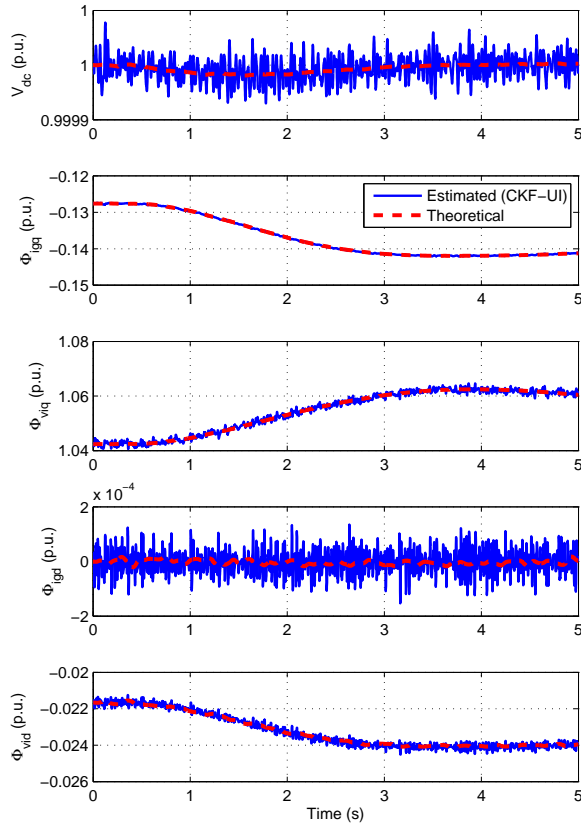


Fig. 16. Case Study 4: Dynamic state estimation results for V_{dc} , Φ_{igq} , Φ_{viq} , Φ_{igd} , and Φ_{vid} .

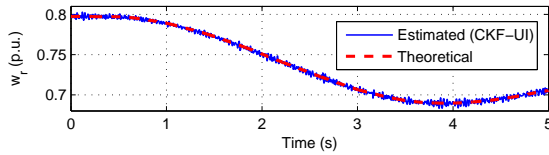


Fig. 17. Case Study 4: Unknown input estimation results for the wind turbine estimation model.

In the above relationship, ξ is a quantity which differs every time step, so as to achieve that $(\zeta - \xi)/(I_{tb}^2 + \xi) = p$, and in our case $p = 0.001$. However, ξ is calculated based on ζ , but, since ζ is a function of $w_r(k-1)$, which is still unknown, the value of the previous time step is used ($w_r(k-2)$), relying on the concept that the value of w_r does not tremendously change in successive time steps. Therefore, ζ_{proxy} is calculated based on $w_r(k-2)$, and, then, ξ is computed, aiming at $(\zeta - \xi)/(I_{tb}^2 + \xi) \approx p$. The factors of $w_r(k-1)$ in (61) are given below:

$$I_t^{ba} = \sqrt{I_{tb}^2 + \xi} - \xi / \left(2\sqrt{I_{tb}^2 + \xi} \right) \quad (96)$$

$$I_{tlina} = I_{lin} / \left(2\sqrt{I_{tb}^2 + \xi} \right) \quad (97)$$

$$I_{tsqa} = I_{sq} / \left(2\sqrt{I_{tb}^2 + \xi} \right) \quad (98)$$

Regarding (52), the same concept is used. From the properties of arctan function, it is $\arctan(a) + \arctan(b) = \arctan((a+b)/(1-ab))$. If $(a+b)/(1-ab) = (I_{sdk} +$

$I_{gdk})/(I_{sqk} + I_{gqk}) = g(w_r)$, then $b = (g(w_r) - a)/(1 + ag(w_r))$, and a can be determined so as for b to be equal to a number close to 0 (which in our case is 0.001), so as to use the first order term only of the standard power series formula for arctan. Thus, the measured value can be used to calculate a (hence considering that $g(w_r) = \tan(\phi_k)$). Therefore, $\phi_k = \arctan(a) + b$, with

$$b = \frac{I_{tdk}^b - aI_{tqk}^b + (K_{Id} - aK_{Iq})w_{r(k-1)}}{I_{tqk}^b + aI_{tdk}^b} \frac{1}{1 + K_w w_{r(k-1)}}$$

where $K_w = (K_{Id} + aK_{Iq})(I_{tqk}^b + aI_{tdk}^b)$, $I_{tdk}^b = I_{sdk}^b + I_{gdk}^b$ and $I_{tqk}^b = I_{sqk}^b + I_{gqk}^b$. The final step is to employ the power series corresponding to $1/(1 + \kappa)$ function, and try to achieve that κ is small, so as to use the first few terms of the series. In a similar way as in the aforementioned $\sqrt{1 + \kappa}$ function:

$$\frac{1}{1 + K_w w_{r(k-1)}} = \frac{1}{1 + \alpha} \frac{1}{1 + \frac{K_w w_{r(k-1)} - \alpha}{1 + \alpha}}$$

In the above relationship, α is calculated, based on that $(K_w w_{r(k-1)} - \alpha)/(1 + \alpha) = 0.001$. Similarly to the I_t case, since $w_r(k-1)$ is unknown, $w_r(k-2)$ is used instead. Hence, the factors of (62), are given as follows:

$$\phi_m = \arctan(a) \quad (99)$$

$$K_{\phi 0} = ((I_{td}^b - aI_{tq}^b)K_{f0}) / (I_{tq}^b + aI_{td}^b) \quad (100)$$

$$K_{\phi i} = \frac{(I_{td}^b - aI_{tq}^b)K_{fi} + (K_{Id} - aK_{Iq})K_{f(i-1)}}{I_{tq}^b + aI_{td}^b}, i = 1, 2, 3 \quad (101)$$

$$K_{\phi 4} = ((K_{Id} - aK_{Iq})K_{f3}) / (I_{tq}^b + aI_{td}^b) \quad (102)$$

where

$$K_{f0} = 1/(1 + \alpha) + \alpha/(1 + \alpha)^2 + \alpha^2/(1 + \alpha)^3 + \alpha^3/(1 + \alpha)^4,$$

$$K_{f1} = -K_w/(1 + \alpha)^2 - 2\alpha K_w/(1 + \alpha)^3 - 3\alpha^2 K_w/(1 + \alpha)^4,$$

$$K_{f2} = K_w^2/(1 + \alpha)^3 + 3\alpha K_w^2/(1 + \alpha)^4, \quad K_{f3} = -K_w^3/(1 + \alpha)^4$$

APPENDIX B DFIG DATA

The DFIG data is listed in the following table.

$L_m = 4,$	$R_s = 0.005,$	$w_s = 1,$	$k_t = 0.3,$	$c = 0.01,$
$H_t = 4,$	$H_g = 0.4,$	$\rho = 1.225,$	$R_t = 40.05,$	$c_1 = 0.5176,$
$c_2 = 116,$	$c_3 = 0.4,$	$c_4 = 0,$	$c_5 = 0,$	$c_6 = 5,$
$c_7 = 21,$	$c_8 = 0.08,$	$c_9 = 0.035,$	$c_{10} = 0.0068,$	$K_{wr} = -150,$
$T_{wr} = 3,$	$T_\beta = 0.5,$	$C_{pmax} = 0.48,$	$\lambda_{opt} = 8.1,$	$R_i = 0,$
$K_{p,Te} = 0,$	$K_{i,Te} = -60,$	$K_{p,iq} = -1,$	$K_{i,iq} = -400,$	
$K_{p,Qs} = 0.5,$	$K_{i,Qs} = 10,$	$K_{p,id} = -0.1,$	$R_g = 0,$	
$K_{i,id} = -20,$	$K_{p,igq} = -22,$	$K_{i,igq} = -870,$	$R_c = 0.7333,$	
$K_{p,viq} = 0.3,$	$K_{i,viq} = 200,$	$K_{p,igd} = 0,$	$K_{i,igd} = -60,$	
$K_{p,vid} = 0.3,$	$K_{i,vid} = 200,$	$L_i = 0.1667,$	$L_g = 0.0033,$	
$C_f = 0.015,$	$V_{dc,ref} = 1,$	$C_{dc} = 2,$	$c_{1,p} = 100,$	
$c_{2,p} = 680,$	$c_{3,p} = 40$			

REFERENCES

- [1] K. Morison, L. Wang, and P. Kundur, "Power system security assessment," *IEEE Power Energy Mag.*, vol. 2, no. 5, pp. 30–39, Sept. 2004.
- [2] P. Panciatici, G. Bareux, and L. Wehenkel, "Operating in the Fog: Security Management Under Uncertainty," *IEEE Power Energy Mag.*, vol. 10, no. 5, pp. 40–49, Sept. 2012.
- [3] C. Taylor, "Improving grid behaviour," *IEEE Spectr.*, vol. 36, no. 6, pp. 40–45, Jun. 1999.
- [4] P. Zhang, F. Li, and N. Bhatt, "Next-Generation Monitoring, Analysis, and Control for the Future Smart Control Center," *IEEE Trans. Smart Grid*, vol. 1, no. 2, pp. 186–192, Sept. 2010.
- [5] S. Wang, W. Gao, and A. Meliopoulos, "An Alternative Method for Power System Dynamic State Estimation Based on Unscented Transformation," *IEEE Trans. Power Syst.*, vol. 27, no. 2, pp. 942–950, May 2012.
- [6] A. Singh and B. Pal, "Decentralized Dynamic State Estimation in Power Systems Using Unscented Transformation," *IEEE Trans. Power Syst.*, vol. 29, no. 2, pp. 794–804, Mar. 2014.
- [7] E. Ghahremani and I. Kamwa, "Dynamic State Estimation in Power System by Applying the Extended Kalman Filter With Unknown Inputs to Phasor Measurements," *IEEE Trans. Power Syst.*, vol. 26, no. 4, pp. 2556–2566, Nov. 2011.
- [8] G. Anagnostou and B. C. Pal, "Derivative-free kalman filtering based approaches to dynamic state estimation for power systems with unknown inputs," *IEEE Transactions on Power Systems*, vol. 33, no. 1, pp. 116–130, Jan 2018.
- [9] R. Huang, R. Diao, Y. Li, J. J. Sanchez-Gasca, Z. Huang, B. Thomas, P. Etingov, S. Kincic, S. Wang, R. Fan, G. H. Matthews, D. Kosterev, S. Yang, and J. Zhao, "Calibrating parameters of power system stability models using advanced ensemble kalman filter," *IEEE Transactions on Power Systems*, vol. PP, no. 99, pp. 1–1, 2017.
- [10] S. Yu, T. Fernando, and H. H. C. Iu, "Dynamic behavior study and state estimator design for solid oxide fuel cells in hybrid power systems," *IEEE Transactions on Power Systems*, vol. 31, no. 6, pp. 5190–5199, Nov 2016.
- [11] K. Emami, H. Ariakia, and T. Fernando, "A functional observer based dynamic state estimation technique for grid connected solid oxide fuel cells," *IEEE Transactions on Energy Conversion*, vol. PP, no. 99, pp. 1–1, 2017.
- [12] S. Yu, K. Emami, T. Fernando, H. H. C. Iu, and K. P. Wong, "State estimation of doubly fed induction generator wind turbine in complex power systems," *IEEE Transactions on Power Systems*, vol. 31, no. 6, pp. 4935–4944, Nov 2016.
- [13] S. Yu, T. Fernando, A. V. Savkin, and H. H. C. Iu, "A dynamic state estimation based sliding mode controller for wind energy generation system connected to multimachine grids," in *2016 IEEE Conference on Control Applications (CCA)*, Sept 2016, pp. 1556–1559.
- [14] S. Yu, T. Fernando, K. Emami, and H. H. C. Iu, "Dynamic state estimation based control strategy for dfig wind turbine connected to complex power systems," *IEEE Transactions on Power Systems*, vol. 32, no. 2, pp. 1272–1281, March 2017.
- [15] S. Yu, T. Fernando, H. H. C. Iu, and K. Emami, "Realization of state-estimation-based dfig wind turbine control design in hybrid power systems using stochastic filtering approaches," *IEEE Transactions on Industrial Informatics*, vol. 12, no. 3, pp. 1084–1092, June 2016.
- [16] L. P. Kunjumammed, B. C. Pal, C. Oates, and K. J. Dyke, "Electrical oscillations in wind farm systems: Analysis and insight based on detailed modeling," *IEEE Transactions on Sustainable Energy*, vol. 7, no. 1, pp. 51–62, Jan 2016.
- [17] F. Mei, "Small-signal modelling and analysis of doubly-fed induction generators in wind power applications."
- [18] S.-K. Chung, "A phase tracking system for three phase utility interface inverters," *IEEE Transactions on Power Electronics*, vol. 15, no. 3, pp. 431–438, May 2000.
- [19] A. Nagliero, R. A. Mastromauro, M. Liserre, and A. Dell'Aquila, "Synchronization techniques for grid connected wind turbines," in *2009 35th Annual Conference of IEEE Industrial Electronics*, Nov 2009, pp. 4606–4613.
- [20] M. Rosyadi, S. M. Muyeen, R. Takahashi, and J. Tamura, "New controller design for pmsg based wind generator with lcl-filter considered," in *2012 XXth International Conference on Electrical Machines*, Sept 2012, pp. 2112–2118.
- [21] L. P. Kunjumammed, B. C. Pal, R. Gupta, and K. J. Dyke, "Stability analysis of a pmsg-based large offshore wind farm connected to a vsc-hvdc," *IEEE Transactions on Energy Conversion*, vol. 32, no. 3, pp. 1166–1176, Sept 2017.

- [22] M. P. Williams, "Solving polynomial equations using linear algebra," *Johns Hopkins APL Technical Digest*, vol. 28, no. 4, pp. 354–363, 2010.
- [23] C. Canizares *et al.*, "Benchmark models for the analysis and control of small-signal oscillatory dynamics in power systems," *IEEE Trans. Power Syst.*, vol. 32, no. 1, pp. 715–722, Jan. 2017.
- [24] "NETS-NYPS 68 Bus System," <http://www.sel.eesc.usp.br/ieee/>.
- [25] "IEEE Standard for Synchrophasor Measurements for Power Systems," *IEEE Std C37.118.1-2011 (Revision of IEEE Std C37.118-2005)*, pp. 1–61, Dec. 2011.
- [26] N. Zhou, D. Meng, Z. Huang, and G. Welch, "Dynamic state estimation of a synchronous machine using pmu data: A comparative study," *IEEE Transactions on Smart Grid*, vol. 6, no. 1, pp. 450–460, Jan 2015.
- [27] M. H. Nawir, "Integration of wind farms into weak AC grids," Ph.D. dissertation, Cardiff University, 2017.
- [28] "Short-Circuit Modeling and System Strength," NERC, White Paper, February 2018, [Online]. Available: https://www.nerc.com/pa/RAPA/ra/Reliability20Assessments20DL/Short_Circuit_whitepaper_Final_1_26_18.pdf.



state estimation, and renewable energy based generation.

Dr. Anagnostou is a member of the Technical Chamber of Greece.

Georgios Anagnostou (M'17) was born in Athens, Greece. He received the Diploma in Electrical and Computer Engineering from the National Technical University of Athens (NTUA), Athens, Greece, the M.Sc. degree in Sustainable Energy Futures from Imperial College London, London, United Kingdom, and the Ph.D. degree in Electrical Engineering from Imperial College London, London, United Kingdom in 2011, 2012, and 2016, respectively. His current research interests include power system dynamics and control, dynamic security assessment, dynamic



2002 to August 2003. In 2006, he joined the Advanced Engineering Group, TVS Motor Company Ltd. Hosur, India, and in 2008, he joined Imperial College London as a Research Assistant. From September 2011 to February 2012, he was with GE Global Research-Europe, Munich, Germany, as a Marie Curie Research Fellow, Secondment from Imperial College London, under the REAL-SMART project funded by the Marie Curie FP7 IAPP scheme. From Dec. 2012 to Jan. 2019 he worked as a Research Associate at Imperial College London. His research interests include power system HVDC networks, power system dynamics, and renewable electricity generation.

Linash P. Kunjumammed (S'01-M'13-SM'16) received the B.Tech. degree from Mahatma Gandhi University, Kottayam, India, the M.S. degree from the Indian Institute of Technology Madras, Chennai, India, and the Ph.D. degree from Imperial College London, London, U.K., in 2002, 2006, and 2012, respectively, all in electrical engineering. He is currently the HVDC Engineer at Mitsubishi Electric Europe, Power System Group - UK. He was a Graduate Apprentice Trainee with Neyveli Lignite Corporation Ltd., Neyveli, India, from September



Vice President Publications, IEEE Power & Energy Society. He was Editor-in-Chief of IEEE Transactions on Sustainable Energy (2012–2017) and Editor-in-Chief of IET Generation, Transmission and Distribution (2005–2012) and is a Fellow of IEEE for his contribution to power system stability and control.

Bikash C. Pal (M'00-SM'02-F'13) received B.E.E. (with honors) degree from Jadavpur University, Calcutta, India, M.E. degree from the Indian Institute of Science, Bangalore, India, and Ph.D. degree from Imperial College London, London, U.K., in 1990, 1992, and 1999, respectively, all in electrical engineering. Currently, he is a Professor in the Department of Electrical and Electronic Engineering, Imperial College London. His current research interests include renewable energy modelling and control, state estimation, and power system dynamics. He is